Post-fault Model of Six-phase PMSMs with an Open-circuit Fault

*Abdolmajid Abedini Mohammadi, Johan Gyselinck, Adrian-Cornel Pop, Samad Taghipour Boroujeni**

Abstract

A post-fault model of six-phase PMSMs with an open-circuit fault is presented. First, the two key properties of the well-known vector space decomposition transformation for the healthy machine, namely decoupling and orthogonality, are discussed. Then a dedicated transformation with similar properties for a faulty machine with one open-circuit fault is derived. It maps the phase domain variables on a new five-dimensional space; the current which builds the magnetomotive force vector in the airgap is mapped on a separate sub-plane, and the currents which do not affect the magnetomotive force vector on the three remaining dimensions called zero-sequence axes. The proposed transformation is generic and can be applied to different star connections, i.e., grounded, connected, and isolated star points. Then, the model of the machine linked with equivalent circuit diagrams is developed. Moreover, the fault-tolerant control of the faulty machine based on the derived faulty model is presented. Simulation results are provided to illustrate the properties of the transformation and show the validity of the proposed model.

Keywords: open-circuit fault, post-fault model, PMSM, six-phase machines, vector space decomposition.

1 Introduction

Six-phase electric machines are an interesting solution for safety-critical applications [1–3]. Thanks to higher redundancy, they can offer higher reliability compared to their three-phase counterparts [4, 5]. Moreover, unlike other multi-phase machines like five- or seven-phase machines [6, 7], they can be supplied with two off-the-shelf three-phase inverters. Additionally, they allow for higher torque density, lower torque ripple, and lower current per phase for given power compared to their three-phase counterparts [8]. The last merit can be attractive for applications with too high phase currents with respect to the converter switches.

Two approaches are developed for modeling six-phase machines in the rotary reference frame in terms of transformed variables [9, 10]. Compared to the phase-domain model, such models can greatly simplify the control of the machine. The six-phase machine can be treated as two three-phase systems, and well-known methods for modeling three-phase machines adopted [11]. Alternatively, the whole winding can be considered as a single entity and Vector Space Decomposition (VSD) transformation is applied [12].

With the first approach, the currents are mapped on two sets of transformed variables; however, magnetic coupling between the two systems occurs; it can hinder the performance of the controller. The latter approach decomposes the current which contributes to energy conversion to just one pair of transformed currents, therefore, as far the torque is related, the control looks like the one of a three-phase machine. However, still there are four currents with zero contribution to the airgap magnetomotive force (MMF), called zero-sequence current hereafter, which can be controlled to achieve other control targets like suppressing current harmonics [8, 13].

In case of open-circuit (OC) fault, the VSD transformation loses some of its benefits because the winding is not balanced anymore. For example, with one OC fault the machine turns basically into a five-phase machine with unbalanced winding; therefore, the quantities relating to the faulty phase are not relevant anymore, as they cannot affect the machine performance. Applying the VSD transformation to the faulty machine still can map the airgap MMF-creating current on a separate plane where the energy conversion occurs (basically the faulty machine can be considered as a healthy machine with zero current at open-circuited phase). However, then the zero-sequence currents automatically take some value and cannot be controlled independently. In mathematical terms, the six transformed variables are not independent anymore.

Because of this current dependency, the fault-tolerant control methods based on the healthy-machine model relies on optimization in order to calculate the reference currents [14–18, 20]. The phase currents are the optimization variables, and minimizing the copper loss and/or extending the range of the

A. Abedini Mohammadi is with AVL software and functions Gmbh, paarstraße 59, 9059, Regensburg, Germany, +4917659104905 (e-mail: abedini_abdolmajid@yahoo.com)

J. Gyselinck is with Université Libre de Bruxelles. His present address is Ecole Polytechnique de Bruxelles Department of Bio, Electro and Mechanical Systems, Electrical Energy group Avenue Franklin Roosevelt 50 (CP165/52), B-1050 Brussels, Belgium phone: +32(0)26502669 (e-mail: johan.gyselinck@ulb.ac.be)

Adrian-Cornel Pop is with Brose Fahrzeugteile GmbH Co. & KG. Würzburg, Germany, Brose, Ohmstraße 2a, 97076 Würzburg, Germany, Phone: +49 931 202 3060 (e-mail: adriancornel.pop@brose.com)

S. Taghipour Boroujeni is with the Department of engineering, Shahrekord University, Shahrekord, Iran, +98(0)9139867245 (e-mail:

torque without violating thermal limits defined as the maximum allowable copper loss are the objectives. The main difference lies in the machine model applied for the optimization problem formulation.

For example, some papers are based on the machine model obtained using the dual-Park transformation [16–19], while some studies use the machine model derived from the VSD transformation [14, 15, 20].

Moreover, the objective function can be defined in different manners. Normally, minimizing the copper loss for given torque is the objective [14]. However, in the case of one or
more OCs, the phase currents do not have necessarily the same amplitude, and at a certain torque, one or more currents reach their nominal value. Therefore, the maximum achievable torque will be limited by the copper losses in the overloaded phases. In order to extend the range of the torque, the optimization can be formulated to have the total copper loss distributed uniformly among the phases; this formulation is known as the maximum torque strategy [14]. Moreover, both of these objectives, i.e., minimum copper loss and maximum range of torque, can be considered at the same time during the optimization; this strategy is called full-range minimum copper loss [15, 21].

The main contribution of this paper lies in proposing a new transformation for a six-phase winding with an OC fault with similar proprieties to the well-known VSD one developed for healthy machine. Such transformations are also presented in [22–25]. However, they are for the machine with isolated stars. The proposed one in this paper is generic and applies to six-phase machines with isolated, connected or grounded star points. Moreover, corresponding equivalent circuit diagrams are derived for different star connections. To the best knowledge of the authors, such diagrams are missing in the literature for the faulty machine. They provide physical insight into operation of the machine in the faulty case. Moreover, the fault tolerant control method based on the faulty machine model is developed. Compared to optimization-based control method, it is more straightforward as it does not require any extra effort to calculate and control non-zero oscillating zero-reference current with minimum control loss strategy.

The VSD transformation is introduced in Section 2, and its essential properties are discussed in Section 3. In section 4, the derivation of the dedicated transformation is detailed. In section 5, the model of a faulty six-phase, permanent magnet synchronous machine (PMSM) is derived. Section 6 presents some simulation cases to prove the validity of the proposed models. Finally, the fault-tolerant control results for both minimum-loss and maximum-torque control strategies are presented.

2 VSD Transformation for Six-phase Winding

The six-phase winding consists of six phases, further referred to as A1, B1, C1, A2, B2, and C2. The phases are arranged into two stars with the phase shift of a 30 $^{\circ}$*elec* (see Figure 1). The VSD transformation maps the phase quantities on six new variables [12]:

$$\begin{pmatrix} X_{\alpha} \\ X_{\beta} \\ X_{z1} \\ X_{z2} \\ X_{o1} \\ X_{o2} \end{pmatrix} = \frac{1}{3} \begin{pmatrix} 1 & \frac{\sqrt{3}}{2} & \frac{-1}{2} & \frac{-\sqrt{3}}{2} & \frac{-1}{2} & 0 \\ 0 & \frac{1}{2} & \frac{\sqrt{3}}{2} & \frac{-1}{2} & \frac{\sqrt{3}}{2} & -1 \\ 1 & \frac{-\sqrt{3}}{2} & \frac{-1}{2} & \frac{\sqrt{3}}{2} & \frac{-1}{2} & 0 \\ 0 & \frac{-1}{2} & \frac{\sqrt{3}}{2} & \frac{1}{2} & \frac{\sqrt{3}}{2} & -1 \\ 1 & 0 & 1 & 0 & 1 & 0 \\ 0 & 1 & 0 & 1 & 0 & 1 \end{pmatrix} \begin{pmatrix} X_{A1} \\ X_{A2} \\ X_{B1} \\ X_{B2} \\ X_{C1} \\ X_{C2} \end{pmatrix} \qquad (1)$$

where X is either phase current, voltage, or flux linkage.

The current which contributes to the airgap MMF is transformed to the $\alpha\beta$ sub-plane, while the currents mapped to the z1z2 and o1o2 sub-planes result in zero MMF in the airgap. Hence, $\alpha\beta$ currents can contribute to energy conversion and torque, while the other currents just lead to extra copper losses.

3 Physical Interpretation of VSD

The VSD transformation has two important properties, namely, decoupling and orthogonality. In order to study the first property, it is useful to calculate the airgap MMF. Assuming sinusoidal distribution for the phase winding, the contribution of each phase to the airgap MMF is [11]:

$$mmf_x(t,\theta) = Ki_x(t)\cos(\theta-\theta_x) \tag{2}$$

where θ *is* the position in the airgap and θ_x is the position of the phase x magnetic axis with respect to an arbitrary reference both in electrical degree, K is a constant proportional to the number of turns per phase. Taking the magnetic axis of phase A1 as the reference, the airgap MMF due to all phases reads:

$$mmf(t,\theta) = Ki_\alpha(t)\cos(\theta) + Ki_\beta(t)\sin(\theta) \tag{3}$$

where

$$i_\alpha(t) = \mathbf{V}_\alpha \mathbf{I}_{\mathrm{ABC}},\ \mathbf{V}_\alpha = \begin{pmatrix} 1 & \frac{\sqrt{3}}{2} & -\frac{1}{2} & -\frac{\sqrt{3}}{2} & -\frac{1}{2} & 0 \end{pmatrix} \tag{4}$$

$$i_\beta(t) = \mathbf{V}_\beta \mathbf{I}_{\mathrm{ABC}},\ \mathbf{V}_\beta = \begin{pmatrix} 0 & \frac{1}{2} & \frac{\sqrt{3}}{2} & \frac{1}{2} & -\frac{\sqrt{3}}{2} & -1 \end{pmatrix} \tag{5}$$

and

$$\mathbf{I}_{\mathrm{ABC}} = \begin{pmatrix} i_{A1}(t) & i_{A2}(t) & i_{B1}(t) & i_{B2}(t) & i_{C1}(t) & i_{C2}(t) \end{pmatrix}^{\mathrm{T}}$$

According to (3), as far as the airgap MMF is related, the dual-star winding is equivalent with a two-phase balanced winding with currents $i_\alpha(t)$ and $i_\beta(t)$ and the same number of turns per phase as the original winding. Indeed, if the airgap MMF is considered as a vector, just two currents flowing in a two-phase winding suffice to define this vector.

$\mathbf{V}_\alpha$ and $\mathbf{V}_\beta$ are the same as the first two rows of the VSD transformation matrix in (1). Therefore, the VSD transformation essentially maps the current producing the airgap MMF to $i_\alpha(t)$ and $i_\beta(t)$. In Figure 2, the corresponding phase currents for given $i_\alpha(t)$ and $i_\beta(t)$ calculated by the inverse VSD transformation are shown in the form of phasor diagrams. It is assumed that $i_\alpha(t)$ and $i_\beta(t)$ form a balanced positive-sequence two-phase system and all other currents are zero. Moreover, all the currents are purely sinusoidal. The phase currents form two balanced, positive-sequence, three-phase systems corresponding to the two stars, where the second system lags the first one by 30 $^\circ$*elec.*.

The case where only i_{z1} and i_{z2} are non-zero is shown in Figure 3. In this case, i_{z1} and i_{z2} form a balanced 2-phase system, however, with negative sequence. Again, the phase currents form two three-phase positive-sequence balanced systems, but the second system lags (leads) the first one by 210 (150) $^\circ$*elec.* (when i_{z1} and i_{z2} are positive-sequence, then the second system leads the first one by 210 $^\circ$*elec.* and the three-phase systems are negative-sequence). The resulting MMFs are [11]:

$$mmf_1(t,\theta) = \frac{3}{2}K\cos(\theta-\omega t) \tag{6}$$

$$mmf_2(t,\theta) = -\frac{3}{2}K\cos(\theta-\omega t) \tag{7}$$

$mmf_1(t,\theta)$ and $mmf_2(t,\theta)$ denote the MMFs of the first and second star, respectively. They are rotating fields with opposite phases. Therefore, the total MMF in the airgap due to i_{z1} and i_{z2} is zero.

Similarly, in Figure 4, the currents for the case with only non-zero i_{o1} and i_{o2} are shown. There is 30 $^\circ$*elec.* phase shift between the two currents (the phase shift is selected randomly). The phase currents in each star have the same phase, but there is a 30 $^\circ$*elec.* phase shift between the currents of the two stars. The phase shift between the currents of the two stars is the same as the one between i_{o1} and i_{o2}. The resulting MMFs are:

$$mmf_1(t,\theta) = mmf_2(t,\theta) = 0 \tag{8}$$

in this case, the phase MMFs in each star sum up to zero.

This simple study illustrates the decoupling property of VSD. It not only provides a better insight into the machine operation but makes the modeling and control simpler as well.

Another important property of the VSD transformation is orthogonality. In order to study this property, it is useful to calculate the magnetic energy stored in the machine. Ignoring saturation, in terms of phase variables, it reads [11]:

$$W_{\mathrm{ABC}}(t)=\frac{1}{2}\mathbf{\Psi}_{\mathrm{ABC}}{}^{\mathrm{T}}\mathbf{I}_{\mathrm{ABC}} \quad (9)$$

where

$$\mathbf{\Psi}_{\mathrm{ABC}}=\begin{pmatrix}\Psi_{\mathrm{A1}}(t) & \Psi_{\mathrm{A2}}(t) & \Psi_{\mathrm{B1}}(t) & \Psi_{\mathrm{B2}}(t) & \Psi_{\mathrm{C1}}(t) & \Psi_{\mathrm{C2}}(t)\end{pmatrix}^{\mathrm{T}}$$

In terms of the transformed variables:

$$W_{\mathrm{VSD}}(t)=\frac{1}{2}\mathbf{\Psi}_{\mathrm{VSD}}{}^{\mathrm{T}}\mathbf{I}_{\mathrm{VSD}} \quad (10)$$

Using the VSD transformation, (10) can be written as:

$$W_{\mathrm{VSD}}(t)=\frac{1}{2}\mathbf{\Psi}^{\mathrm{T}}\mathbf{T}^{\mathrm{T}}\mathbf{T}\mathbf{I} \quad (11)$$

with $\mathbf{T}$ the VSD transformation matrix of (1). The energies obtained according to (9) and (11) are equal, when the following condition is fulfilled:

$$\mathbf{T}^{\mathrm{T}}\mathbf{T}=\mathbf{I}_6 \quad (12)$$

with $\mathbf{I}_6$ the 6×6 identity matrix. Equation (12) implies that $\mathbf{T}$ is an orthogonal matrix. It means:

$$\begin{cases} v_{\mathrm{i}}.v_{\mathrm{j}}=0 & for\, i\neq j \\ v_{\mathrm{i}}.v_{\mathrm{i}}=1 & \end{cases} \quad (13)$$

where v is one column or row of the transformation and i,j = 1,2,..6. It can be concluded that the orthogonality guarantees that the machine models based on phase and transformed variables are equivalent (for example the torque calculated using both models are the same).

4 Dedicated Transformation with One OC

When there is a phase OC fault in a dual-star machine, the variables related to the faulty phase are not relevant anymore. Hence, it can be considered a five-phase machine with unbalanced winding. In this section, a dedicated transformation for the faulty machine with one OC fault is derived.

Without loss of generality, it is assumed that phase C2 is open-circuited. The machine winding configuration after the fault is shown in Figure 5. Similar to the healthy machine, the airgap MMF is calculated as:

$$mmf(t,\theta)= K\left(i_{\alpha}(t)\cos(\theta)+i_{\beta}(t)\sin(\theta)\right) \quad (14)$$

where

$$i_{\alpha}(t)=\mathbf{V}_{\alpha f}\mathbf{I}_{\mathrm{f}},\ \mathbf{V}_{\alpha f}=\begin{pmatrix}1 & \frac{\sqrt{3}}{2} & -\frac{1}{2} & -\frac{\sqrt{3}}{2} & -\frac{1}{2}\end{pmatrix} \quad (15)$$

$$i_{\beta}(t)=\mathbf{V}_{\beta f}\mathbf{I}_{\mathrm{f}},\ \mathbf{V}_{\beta f}=\begin{pmatrix}0 & \frac{1}{2} & \frac{\sqrt{3}}{2} & -\frac{1}{2} & -\frac{\sqrt{3}}{2}\end{pmatrix} \quad (16)$$

and $\mathbf{I}_{\mathrm{f}}=\begin{pmatrix}i_{A1}(t) & i_{A2}(t) & i_{B1}(t) & i_{B2}(t) & i_{C1}(t)\end{pmatrix}^{\mathrm{T}}$.

Similar to the healthy machine, according to (14), the airgap MMF can be represented by i_α and i_β flowing in a two-phase balanced winding. Moreover, the two vectors are orthogonal.

The phase currents of the faulty machine span a five-dimensional space. Therefore, the dimension of the dedicated matrix needs to be 5×5. Taking $\mathbf{V}_{\alpha f}$ and $\mathbf{V}_{\beta f}$ as the first two rows of the matrix, the three others need to be selected. If these rows are selected as vector of currents which lead to zero MMF, they will be orthogonal with $\mathbf{V}_{\alpha f}$ and $\mathbf{V}_{\beta f}$. Similar to the healthy machine, when the currents in the three phases of the healthy star are the same while other currents are zero, the resulting MMF will be zero. Therefore, i_{o1} can be defined as:

$$i_{o1}(t) = \mathbf{V}_{of}\mathbf{I}_f\,, \quad \mathbf{V}_{of} = \begin{pmatrix} 1 & 0 & 1 & 0 & 1 \end{pmatrix} \tag{17}$$

In order to have zero MMF in the airgap, the two other current vectors should meet the following conditions:

$$i_\alpha(t) = i_\beta(t) = 0 \tag{18}$$

with $i_\alpha(t)$ and $i_\beta(t)$ defined in (15) and (16). It means:

$$\begin{aligned} & i_{A1}(t) + \frac{\sqrt{3}}{2} i_{A2}(t) - \frac{1}{2} i_{B1}(t) - \frac{\sqrt{3}}{2} i_{B2}(t) - \frac{1}{2} i_{C1}(t) = 0 \\ & \frac{1}{2} i_{A2}(t) + \frac{\sqrt{3}}{2} i_{B1}(t) + \frac{1}{2} i_{B2}(t) - \frac{\sqrt{3}}{2} i_{C1}(t) = 0 \end{aligned} \tag{19}$$

Moreover, when the sum of the currents of the first star is zero, i.e., $i_{A1}(t)+i_{B1}(t)+i_{C1}(t)=0$, these two vectors will be orthogonal with $\mathbf{V}_o$. By applying this condition, (19) can be simplified to:

$$\begin{aligned} & \frac{3}{2} i_{A1}(t) + \frac{\sqrt{3}}{2} i_{A2}(t) - \frac{\sqrt{3}}{2} i_{B2}(t) = 0 \\ & \frac{\sqrt{3}}{2} i_{A1}(t) + \frac{1}{2} i_{A2}(t) + \sqrt{3} i_{B1}(t) + \frac{1}{2} i_{B2}(t) = 0 \end{aligned} \tag{20}$$

Eq. (20) consists of two equations with four unknowns. It can be written in terms of two new currents. Let us define two new currents as function of i_{A2} and i_{B2}:

$$\begin{pmatrix} i_x(t) \\ i_y(t) \end{pmatrix} = \begin{pmatrix} a & b \\ c & d \end{pmatrix} \begin{pmatrix} i_{A2}(t) \\ i_{B2}(t) \end{pmatrix} \tag{21}$$

Using (20) and (21), all phase currents can be calculated as a function of $i_x(t)$ and $i_y(t)$ as follows:

$$\begin{pmatrix} i_{A1}(t) \\ i_{A2}(t) \\ i_{B1}(t) \\ i_{B2}(t) \\ i_{C1}(t) \end{pmatrix} = \frac{1}{ad-bc} \begin{pmatrix} -\frac{\sqrt{3}}{3}(d+c) & \frac{\sqrt{3}}{3}(a+b) \\ d & -b \\ \frac{\sqrt{3}}{3}c & -\frac{\sqrt{3}}{3}a \\ -c & a \\ \frac{\sqrt{3}}{3}d & -\frac{\sqrt{3}}{3}b \end{pmatrix} \begin{pmatrix} i_x(t) \\ i_y(t) \end{pmatrix} \tag{22}$$

The two columns of the 5×2 matrix above can be considered as two vectors of currents for which the airgap MMF is zero:

$$i_{z1}(t) = \frac{1}{ad-bc} \begin{pmatrix} -\frac{\sqrt{3}}{3}(d+c) & d & \frac{\sqrt{3}}{3}c & -c & \frac{\sqrt{3}}{3}d \end{pmatrix} \mathbf{I}_f \tag{23}$$

$$i_{z2}(t) = \frac{1}{ad-bc} \begin{pmatrix} \frac{\sqrt{3}}{3}(a+b) & -b & -\frac{\sqrt{3}}{3}a & a & -\frac{\sqrt{3}}{3}b \end{pmatrix} \mathbf{I}_f \tag{24}$$

For the orthogonality of these two vectors, the following condition should be satisfied:

$$\frac{5}{3} d * b + \frac{5}{3} c * a + \frac{1}{3} d * a + \frac{1}{3} c * b = 0 \tag{25}$$

There are an infinite number of solutions for (25), as there are four unknowns with just one equation. One solution is $a=-b=1$ and $c=d=1$, producing:

$$i_{z1}(t)=\mathbf{V}_{zf1}\mathbf{I}_{\mathrm{f}},\ \mathbf{V}_{zf1}=\begin{pmatrix}-\frac{\sqrt{3}}{2} & \frac{1}{2} & \frac{\sqrt{3}}{6} & -\frac{1}{2} & -\frac{\sqrt{3}}{6}\end{pmatrix} \quad (26)$$

$$i_{zf2}(t)=\mathbf{V}_{zf2}\mathbf{I}_{\mathrm{f}},\ \mathbf{V}_{zf2}=\begin{pmatrix}0 & \frac{1}{2} & -\frac{\sqrt{3}}{6} & \frac{1}{2} & \frac{\sqrt{3}}{6}\end{pmatrix} \quad (27)$$

The dedicated VSD transformation for the faulty machine with single OC at Phase C2 can be built by assembling all the vectors, namely $\mathbf{V}_{\alpha\mathrm{f}}$, $\mathbf{V}_{\beta\mathrm{f}}$, $\mathbf{V}_{\mathrm{zf1}}$, $\mathbf{V}_{\mathrm{zf2}}$, and $\mathbf{V}_{\mathrm{of}}$, as the rows of the matrix. Moreover, according to (13) in order to have an orthogonal matrix, the vectors should be normalized:

$$\begin{pmatrix}X_{\alpha}\\X_{\beta}\\X_{z1}\\X_{z2}\\X_{o1}\end{pmatrix}=\begin{pmatrix}\frac{\sqrt{3}}{3} & \frac{1}{2} & \frac{-\sqrt{3}}{6} & \frac{-1}{2} & \frac{-\sqrt{3}}{6}\\ 0 & \frac{-\sqrt{2}}{4} & \frac{\sqrt{6}}{4} & \frac{\sqrt{2}}{4} & \frac{-\sqrt{6}}{4}\\ \frac{-\sqrt{3}}{3} & \frac{1}{2} & \frac{\sqrt{3}}{3} & \frac{-1}{2} & \frac{\sqrt{3}}{3}\\ 0 & \frac{\sqrt{6}}{4} & \frac{-\sqrt{2}}{2} & \frac{\sqrt{6}}{4} & \frac{-\sqrt{2}}{2}\\ \frac{\sqrt{3}}{3} & 0 & \frac{\sqrt{3}}{3} & 0 & \frac{\sqrt{3}}{3}\end{pmatrix}\begin{pmatrix}X_{A1}\\X_{A2}\\X_{B1}\\X_{B2}\\X_{C1}\end{pmatrix} \quad (28)$$

It should be noted that thanks to orthogonality, the above transformation is power-invariant. The amplitude-invariant version cannot be defined because with the unbalanced winding, the currents do not necessarily form a balanced system even under fault-tolerant control.

5 Model of Six-phase PMSMs with One OC

In this section, the model of the machine with one OC at phase C2 based on the proposed transformation is derived. The voltage equations in the phase domain are:

$$v_x=ri_x+\frac{d}{dt}\psi_x,\qquad x\in\{\mathrm{A1,B1,C1,A2,B2}\} \quad (29)$$

where v, i, ψ *are* phase voltage, current, and flux linkage, respectively, and r is the phase resistance. The latter is assumed to be the same among all phases. Phase C2 equation is irrelevant.

By transforming (29) using (28), the voltage equations in terms of the transformed variables are obtained as:

$$V_x=ri_x+\frac{d}{dt}\psi_x,\qquad x\in\{\alpha,\beta,\mathrm{z1,z2,o1}\} \quad (30)$$

If it is assumed that the phase winding distributions are purely sinusoidal, the stator and rotor magnetic steel is linear, the PM flux linkages with phase winding are sinusoidal, and the mutual flux leakage of phases is zero, the self- and mutual-inductance of the phase winding can be expressed as [11]:

$$L_{xx}=L_l+L_{mA}+L_{mB}\cos(2\theta_x) \quad (31)$$

$$M_{xy}=L_{mA}\cos(\theta_x-\theta_y)+L_{mB}\cos(\theta_x-\theta_y)\ \text{for}\ x\neq y \quad (32)$$

where $x,y\in\{\mathrm{A1,B1,C1,A2,B2}\}$, L_l is the leakage inductance of the phase and θ_x and θ_y are the electrical angular positions of the rotor d-axis with respect to the magnetic axes of phases x and y, respectively. L_{mA} is the average value of magnetizing inductance and L_{mB} the amplitude of its variation with rotor position. With cylindrical rotor, L_{mB} is zero. It should be noted that the inductance harmonics greater than 2 are ignored.

As there are five phases, the size of the inductance matrix is 5×5, containing 5 self-inductances and 20 mutual inductances. Based on the above assumptions, the relationship between phase currents and flux linkages can be written as:

$$\mathbf{\Psi} = \mathbf{LI} + \mathbf{\Psi}_{\mathrm{PM}} \tag{33}$$

where $\mathbf{L}$ is the inductance matrix, $\mathbf{\Psi}, \mathbf{I}$ and $\mathbf{\Psi}_{\mathrm{PM}}$ are the vectors of the phase flux linkages, the phase currents, and the phase PM flux linkages, respectively. The phase PM flux linkage can be represented as:

$$\Psi_{\mathrm{PMx}} = \Psi_{\mathrm{PM}} \cos\left(\theta_{\mathrm{x}}\right) \tag{34}$$

where ψ_{PM} is the amplitude of the PM flux linkage, which is the same for all phases.

Assuming the magnetic axis of Phase A1 as the reference, the flux linkage equations in the phase domain in (33) can be transformed by (28) (Both sides of (33) are multiplied by the coefficient matrix in (28)):

$$\begin{pmatrix} \Psi_\alpha \\ \Psi_\beta \\ \Psi_{z1} \\ \Psi_{z2} \\ \Psi_{o1} \end{pmatrix} = \begin{pmatrix} \mathbf{Q} + L_l \mathbf{I}_2 & 0 \\ 0 & L_l \mathbf{I}_3 \end{pmatrix} \begin{pmatrix} i_\alpha \\ i_\beta \\ i_{z1} \\ i_{z2} \\ i_{o1} \end{pmatrix} + \begin{pmatrix} \sqrt{3}\Psi_{PM} cos\theta_r \\ \sqrt{2}\Psi_{PM} sin\theta_r \\ 0 \\ 0 \\ 0 \end{pmatrix}. \tag{35}$$

$$\mathbf{Q} = \begin{pmatrix} 3L_{mA} + 3L_{mB}\cos 2\theta_r & \sqrt{6}L_{mB}\sin 2\theta_r \\ \sqrt{6}L_{mB}\sin 2\theta_r & 2L_{mA} - 2L_{mB}\cos 2\theta_r \end{pmatrix}$$

where θ_r is the rotor position with respect to the magnetic axis of Phase A1 in electrical degree and $\mathbf{I}_n$ is the *n*x*n* identity matrix.

The flux linkages of different axes are decoupled, except for the coupling between α and β axes which is caused by the magnetic saliency of the rotor like the healthy machine. Moreover, the flux linkages due to PMs and the airgap MMF are mapped just to $\alpha\beta$ sub-plane and form an orthogonal two-phase system.

The voltage equations in terms of equivalent inductances can be obtained from (30) and (35). For the sake of simplicity, let us for now ignore the magnetic saliency of the rotor, i.e., $L_{mB} = 0$. Then, the voltage equations read:

$$V_\alpha = ri_\alpha + \left(L_l + 3L_{mA}\right)\frac{d}{dt}i_\alpha - \sqrt{3}\omega\Psi_{PM} sin\theta_r \tag{36}$$

$$V_\beta = ri_\beta + \left(L_l + 2L_{mA}\right)\frac{d}{dt}i_\beta + \sqrt{2}\omega\Psi_{PM} cos\theta_r \tag{36}$$

$$V_x = ri_x + L_l\frac{d}{dt}i_x, \quad x \in \{\mathrm{z1, z2, o1}\} \tag{37}$$

where ω is the angular speed of the rotor in electrical rad/s.

The $\alpha\beta$ voltage equations are not balanced; the magnetizing inductances ($3L_{mA}$ and $2L_{mA}$) and the amplitude of flux linkages due to the PMs are not the same. The voltage equations relating to the z1, z2, and o1 axes are identical to the healthy machine. The machine model is shown in Figure 6.

Applying the Park transformation to $\alpha\beta$ voltage equations in (36) and (37) produces more complex equations because the unbalance. In this regard, it is useful to define substitute variables for the β-axis variables, i.e.,:

$$V_\beta^{'} = \sqrt{\frac{3}{2}}V_\beta, \; i_\beta^{'} = \sqrt{\frac{2}{3}}i_\beta \tag{39}$$

The squared of the voltage coefficient in (39) is equal to the ratio of the α-axis over β-axis magnetizing inductance in (36) and (37). It is equivalent to referring the β-axis equation to the primary winding of an ideal transformer with turn ratio √3:√2.

The machine model in $\alpha\beta$ sub-plane is shown in Figure 7.

The β-axis voltage equation in terms of the substitute variables is:

$$V'_{\beta} = r'i'_{\beta} + \left(L'_{l} + 3L_{mA}\right)\frac{d}{dt}i'_{\beta} + \sqrt{2}\omega\Psi_{PM}cos\theta_{r} \quad (40)$$

with $r' = \frac{3}{2}r$ and $L'_l = \frac{3}{2}L_l$. In terms of the new variables, the magnetizing inductances of the two axes are the same and the PM flux linkages form a balanced two-phase system.

Applying the Park transformation to voltage equations in $\alpha\beta$ sub-plane in terms of substitute variables (with $L_{mB} \neq 0$) gives:

$$\begin{pmatrix} V_d \\ V_q \end{pmatrix} = \begin{pmatrix} V_{dh} \\ V_{qh} \end{pmatrix} + \begin{pmatrix} V_{df} \\ V_{qf} \end{pmatrix} \quad (41)$$

$$\begin{pmatrix} V_{dh} \\ V_{qh} \end{pmatrix} = r\begin{pmatrix} i_d \\ i_q \end{pmatrix} + \begin{pmatrix} sL_D & -\omega L_Q \\ \omega L_D & sL_Q \end{pmatrix}\begin{pmatrix} i_d \\ i_q \end{pmatrix} + \omega\begin{pmatrix} 0 \\ \sqrt{3}\Psi_{PM} \end{pmatrix}$$

$$L_D = L_l + 3L_{mA} + 3L_{mB} \quad (42)$$

$$L_Q = L_l + 3L_{mA} - 3L_{mB}$$

$$\begin{pmatrix} V_{df} \\ V_{qf} \end{pmatrix} = \left(\frac{L_l}{2}\begin{pmatrix} \frac{\sin(2\theta_{r)}}{2} & -sin^2\theta_r \\ cos^2\theta_r & -\frac{\sin(2\theta_{r)}}{2} \end{pmatrix} + (r' - r)\mathbf{C} + \left(L_l^{'} - L_l\right)\mathbf{C}s \right)\begin{pmatrix} i_d \\ i_q \end{pmatrix} \quad (43)$$

$$\mathbf{C} = \begin{pmatrix} sin^2\theta_r & \frac{\sin(2\theta_{r)}}{2} \\ \frac{\sin(2\theta_{r)}}{2} & cos^2\theta_r \end{pmatrix}$$

s denotes time derivation operator. (Eq. 42) is the same as the voltage equations of the healthy six-phase machine. Eq. (43) represents the extra voltage terms introduced because of the fault. They depend on the phase resistance, leakage inductance, and rotor position.

As far as the machine control is related, the voltage terms in (43) which are just a function of current (the first two terms) affect the steady state response and can be compensated by a feed-forward network. The last term in (43) affects the transient response and cannot be compensated easily because it includes the time derivative of currents. Assuming that the leakage inductance is relatively small, its effect on the transient response can be ignored. Moreover, because the same inductance as in the healthy-machine case appears in the first four terms, the same controller can be used for both healthy and faulty machines.

The machine torque reads:

$$T = \frac{\partial W}{\partial \theta_r} = p\left(\Psi_d i_q - \Psi_q i_d\right) \quad (44)$$

where W is given by (9). Ψ_d and Ψ_q are the flux linkages obtained by transforming Ψ_α and Ψ'_β to the synchronous frame:

$$\begin{pmatrix} \Psi_d \\ \Psi_q \end{pmatrix} = \begin{pmatrix} L_D & 0 \\ 0 & L_Q \end{pmatrix}\begin{pmatrix} i_d \\ i_q \end{pmatrix} + \begin{pmatrix} \sqrt{3}\Psi_{PM} \\ 0 \end{pmatrix} + \left(L_l^{'} - L_l\right)\mathbf{C} \quad (45)$$

Eq. (44) is essentially the same as the torque equation for the healthy machine obtained based on the power-invariant VSD transformation.

5.1 Isolated Star Points

The introduced model applies to the general case where the two-star points are grounded (zero-sequence currents can flow independently in the two stars). In the case that the two-star points are isolated, the sum of the currents in the first star is always zero, and therefore $i_{o1} = 0$. Moreover, the currents of the two healthy phases of the second star are always equal with a negative sign, i.e., $i_{A2} = -i_{B2}$. According to (28), we obtain:

$$i_{z2} = -\frac{\sqrt{3}}{3} i_\beta \tag{46}$$

Then, $V_\beta^{'}$ can be defined as (47).

$$V_\beta^{'} = \sqrt{\frac{3}{2}}\left(V_\beta - \frac{\sqrt{3}}{3} V_{z2}\right) = r' i'_\beta + \left(L'_l + 3L_{mA}\right)\frac{d}{dt} i'_\beta + \sqrt{2}\omega \Psi_{PM} cos\theta_r \tag{47}$$

With isolated star points $r' = 2r$ and $L_l' = 2L_l$. The voltage equations of the α and z1 axes remain the same, and the z2 and o1 axes ones are not relevant anymore. The machine model with two isolated star points is shown in Figure 8 (a).

5.2 Connected Star Points

With two connected star points, the sum of the phase currents must be zero. In terms of transformed variables, it means:

$$\sqrt{6} i_{o1} + \sqrt{3} i_{z2} + i_\beta = 0 \tag{48}$$

It is useful to define a new current as:

$$i_{circ} = 2\sqrt{3} i_{z2} - \sqrt{6} i_{o1} \tag{49}$$

Based on the (48) and (49), the voltage equations can be rewritten as:

$$V_\beta^{'} = \sqrt{\frac{3}{2}}\left(V_\beta - \frac{\sqrt{3}}{9} V_{z2} - \frac{\sqrt{6}}{9} V_{O1}\right) = r' i'_\beta + \left(L'_l + 3L_{mA}\right)\frac{d}{dt} i'_\beta + \sqrt{2}\omega \Psi_{PM} cos\theta_r \tag{50}$$

$$V_{circ} = 2\sqrt{3} V_{z2} - \sqrt{6} V_{o1} = r i_{circ} + L_l \frac{d}{dt} i_{circ} \tag{51}$$

With connected star points $r' = \frac{5}{3} r$ and $L_l' = \frac{5}{3} L_l$. The z1 axis voltage equation remains the same. The machine model with connected neutral points and one OC at phase C2 based in (50) and (51) is shown in Figure 8 (b).

6 Simulation Results and Fault-tolerant Control

In this section, the simulation results for the control of the machine with one OC fault at Phase C2 based on the model presented in the previous section is implemented.

The electrical parameters of the six-phase PMSM modeled in this section are included in Table 1. The cross-section of the machine is shown in Figure 9. The stator has 12 teeth and there are 10 poles on the rotor side with interior PMs. The stator winding is made up of 2 stars shifted by 30 °*elec.*. The phase and coil directions are shown on the coil sides by letters corresponding to the phases. The outer surface of the rotor is shaped in order to minimize the cogging torque of the machine. More information about the machine including geometrical parameters can be found in [8].

For emulating the OC fault, the dual-star machine model is implemented in the phase domain, and a large-value resistor is connected in series with Phase C2. The reference currents or voltages are calculated based on the transformation in (28) and equations in Section 5. The control structure applies simple PI controllers for dq currents and single-phase controller [27, 28] for zero-sequence currents.

The simulations are conducted using MATLAB/SIMULINK. The block diagram of the controller is shown in Figure 10. The measured phase currents are decoupled using the proposed transformation in (28) into $\alpha\beta$ sub-plane and z1, z2, and o1 axes.

The β-axis current is referred to the primary winding of the transformer shown in Figure 7. Then, similar to the healthy machine, the DQ currents are fed as the input to the PI controller. Finally, the calculated reference voltages are referred back to the secondary winding of the transformer, and using the inverse of the proposed transformation, the corresponding reference phase voltages are calculated.

The feed-forward network is used in order to decouple D and Q-axis voltage equations. It is shown in Figure 10 (b) for the case with two grounded neutral points. Besides the term for compensating the induced voltage because of D- and Q-axis flux linkages, there are two extra terms for compensating the coupling because of the phase resistance and leakage inductance according to (41). These two terms depend on the rotor position. It should be noted that with isolated and connected star points, these two terms need to be multiplied by factors 2 and 4/3 according to equations (47) and (50), respectively. The z1, z2, and o1 currents are controlled separately using three single-phase controllers. The block diagram of the controller is shown in Figure 10 (c).

In order to study the decoupling property of the dedicated transformation, the simulation results for the machine with two grounded star points are shown in Figure 11 (a). The reference dq currents are selected for nominal torque. All currents are normalized with respect to their maximum value at healthy operation. Moreover, the same reference as for $\alpha\beta$ currents is used for normalizing z1-, z2-, and o1- axis currents. i_{z1}, i_{z2}, and i_{o1} are supplied at 0.1 s, 0.15 s. and 0.2 s, receptively. The phase and amplitude of the currents are selected randomly. Upon injecting these currents, the torque remains the same and no disturbance on i_α and $i_{\beta 0}$ is observed. It clearly shows the decoupling effect of the transformation.

The effect of the feed-forward voltages for compensation of the coupling terms between the d- and q-axis because of the resistance and leakage inductance (see (41)) is shown in Figure 11 (b). The simulation results are for the case with connected star points. Moreover, all zero-sequence currents are zero. The feed-forward voltages proportional to the leakage inductance and resistance are supplied at 0.1 s and 0.15 s, respectively. The voltages are normalized with respect to the maximum value of the phase BEMF. It can be observed that upon supplying the feed-forward voltages, the ripple in the dq currents reduces, and consequently the torque ripple decreases. Finally, when both voltages are fed to the machine, the ripple in the dq currents and torque is totally removed.

In order to study the effect of leakage inductance on the coupling between d- and q-axis during the transient period, the step response of the controller is shown in Figure 12. The two star points are isolated, and the step response of the q-axis current for two different cases is studied. In Figure 12 (a), the step response for the original value of the leakage inductance is shown. Unlike the healthy-machine case, the i_q deviates from the first-order closed-loop system response. Some overshoot in the current and subsequently torque is observed and, moreover, i_d is affected during the transient period. This occurs because of the uncompensated coupling between the d- and q-axis in terms of current derivative caused by the leakage inductance (see (43)). In Figure 12 (b), similar results with leakage inductance reduced by a factor of 10 so that its effect on the transient response diminishes are shown. In this case, the step response is much closer to the one of a first-order system, and the overshoot in the torque and current is mush smaller compared to the previous case.

Thanks to the dedicated transformation, when the zero-axis currents are zero, the control corresponds to the minimum-loss strategy. Unlike the optimization-based fault-tolerant control approach which relies on the healthy machine model, there is no need to assign any reference value to the zero-sequence currents. However, in order to switch to maximum-torque strategy, the proper zero-axis reference currents should be supplied. They can be obtained using an optimization algorithm as discussed in [14, 15, 20]. In Figure 13, simulation results for these two control strategies with connected or isolated star points are shown. The control strategy is switched from minimum-loss to maximum-torque at 0.1 s. With the maximum-torque strategy the peak of the phase currents are equal and the total copper loss distributed uniformly among phases. However, because of the zero-axis currents, the total copper loss increases.

7 Conclusion

A dedicated transformation for a faulty six-phase PMSM machine with one OC fault is developed. It offers similar advantages like VSD one for the healthy machine. Moreover, it provides clear insight into operation of the faulty machine. The derived transformation is general and can be applied for various 6-phase winding diagrams in terms of connection of the two star points. Although in this paper the model of a six-phase faulty PMSM is obtained, the transformation can be used for other types of six-phase machines like inductions ones. The control concept of the machine based on the new transformation using PI controllers and feed-forward network was developed. It was shown that the control corresponds to minimum loss control strategy while the zero-sequence currents are zero. Compared to optimization-based fault tolerant control methods, it does not need any extra effort to calculate required zero-sequence currents. However, Additionally, similar methodology like what detailed out in this paper for a six-phase machine can be applied to derive corresponding transformations for other multi-phase winding at faulty operation.

Acknowledgements

This work has been carried out in the frame of the INTERACT project which has received funding from the European Union Horizon 2020 (grant agreement No 766180). Moreover, the authors would like to thank Brose Fahrzeugteile GmbH Co. & KG. Würzburg, Germany for supporting this work.

References

[1] M. Alemi-Rostami, G. Rezazadeh, F. Tahami, et al., "Fault-tolerant capability analysis of six-phase induction motor with distributed, concentrated and pseudo-concentrated windings," *Scientia Iranica,* **31**(10), pp. 775-789 (2022) DOI: 10.24200/SCI.2022.58674.5844

[2] A. G. Yepes, O. Lopez, I. Gonzalez-Prieto, et al., "A comprehensive survey on fault tolerance in multiphase ac drives, part 1: General overview considering multiple fault types," Machines, **10**(3), pp. 1-134 (2022), DOI: 10.3390/machines10030208.

[3] A. G. Yepes, I. Gonzalez-Prieto, O. Lopez, et al., "A comprehensive survey on fault tolerance in multiphase ac drives, part 2: Phase and switch open-circuit faults," Machines, **10**(3), pp. 1-78 (2022), DOI: 10.3390/machines10030221.

[4] Parsa, Leila. "On advantages of multi-phase machines." *31st Annual Conference of IEEE Industrial Electronics Society*, New York City, (2005) **DOI:** 10.1109/IECON.2005.1569139

[5] E. Levi, "Multiphase electric machines for variable-speed applications," IEEE Trans. Ind. Electron, **55**(5), pp. 1893–1909, (2008), **DOI:** 10.1109/TIE.2008.918488.

[6] Z. Heidari, H. Gorginpour, and M. Shahparasti, "Optimal electromagnetic-thermal design of a seven-phase induction motor for high-power speed-control applications," Scientia Iranica, **29**(5), pp. 2480–2497, (2022) DOI: 10.24200/SCI.2021.54766.4028

[7] H. Pairo and M. Farzi, "A look-up table based method for voltage balancing of neutral-point in five-level anpc converter," Scientia Iranica, 2023 DOI: 10.24200/SCI.2023.59080.6050

[8] A. A. Mohammadi, S. Ciceo, Y. Mollet, et al, "Comparative analysis of single-star and dual-star permanent-magnet synchronous machines," *18th International Conference on Electrical Machines, Gothenburg* (2020), DOI: 10.1109/ICEM49940.2020.9270758

[9] A. A. Mohammadi, J. Gyselinck, and A.-C. Pop, "Dynamic modeling of dual-star permanent-magnet synchronous machines using look-up tables," *Electric Vehicles International Conference*, Bucharest (2019) DOI: 10.1109/EV.2019.8893137

[10] A. Abedini Mohammadi, "Fault-tolerant control and robust design of dual-star PMSMs for power steering systems," Ph.D. dissertation, Université libre de Bruxelles (ULB), Brussels, Belgium, (2022).

[11] P. C. Krause, O. Wasynczuk, S. D. Sudhoff, et al., "*Analysis of electric machinery and drive systems", In electric Machines and drives,* pp.160-215, John Wiley & Sons, (2013)

[12] Y. Zhao and T. A. Lipo, "Space vector pwm control of dual three-phase induction machine using vector space decomposition," *IEEE Transactions on industry applications*, **31**(5), pp. 1100–1109 (1995), DOI: 10.1109/28.464525.

[13] S. Taghipour Boroujeni, S. P. Emami, N. Takorabetet al., "Torque ripple minimization in consequent-pole pm machines using harmonic current injection," *Scientia Iranica*, (2022) DOI: 10.24200/SCI.2022.60312.6725

[14] H. S. Che, M. J. Duran, E. Levi, et al., "Postfault operation of an asymmetrical six-phase induction machine with single and two isolated neutral points," *IEEE Trans. Pow. Electron*, **29**(10), pp. 5406–5416, (2013) DOI: 10.1109/TPEL.2013.2293195.

[15] F. Baneira, J. Doval-Gandoy, A. G. Yepes,et al "Control strategy for multiphase drives with minimum losses in the full torque operation range under single open-phase fault," *IEEE Trans. Pow. Electron*, **32**(8), pp. 6275–6285, (2016) DOI: 10.1109/TPEL.2016.2620426

[16] W. Wang, J. Zhang, M. Cheng, et al., "Fault tolerant control of dual three-phase permanent-magnet synchronous machine drives under open-phase faults," *IEEE Trans. Pow. Electron*, **32**(3), pp. 2052–2063, (2016) DOI: 10.1109/TPEL.2016.2559498

[17] G. Feng, C. Lai, W. Li, et al., "Open phase fault modeling and optimized fault-tolerant control of dual three-phase permanent magnet synchronous machines," *IEEE Trans. Pow. Electron*, **34**(11), pp. 11116–11127, (2016) DOI:, 10.1109/TPEL.2019.2900599

[18] W. Li, G. Feng, Z. Li, et al., "Multireference frame based open-phase fault modeling and control for asymmetrical six-phase interior permanent magnet motors," *IEEE Trans. Pow. Electron*, **36**(10), pp11712–11725, (2021) DOI: 10.1109/TPEL.2021.3072947

[19] M.-A. Shamsi-Nejad, B. Nahid-Mobarakeh, S. Pierfederici, et al., "Fault tolerant and minimum loss control of double-star synchronous machines under open phase conditions," *IEEE Trans. Ind. Electron*, **55**(5), pp. 1956–1965, (2008) DOI:, 10.1109/TIE.2008.918485

[20] A. G. Yepes, J. Doval-Gandoy, F. Baneira, et al., "Control strategy for dual three-phase machines with two open phases providing minimum loss in the full torque operation range," *IEEE Trans. Pow. Electron*, **33**(12), pp. 10044–10050 (2018) DOI :. 10.1109/TPEL.2018.2830507

[21] G. Yang, H. Hussain, S. Li, J. Zhang, et al, “A unified fault-tolerant strategy for multiphase machine with minimum losses in full torque operation range based on closed-form expressions,” *IEEE Trans. Pow. Electron*, **37**(10), pp. 12463–12473, (2022) DOI: 10.1109/TPEL.2022.3172389

[22] Y. Zhao and T. A. Lipo, “Modeling and control of a multi-phase induction machine with structural unbalance,” *IEEE Trans. Energy Convers*, **11**(3), pp. 578–584 (1996) DOI: 10.1109/60.537028

[23] Y. Hu, Z. Zhu, and Z.-y. Wu, “Modelling and vector control of dual three-phase pmsm with one-phase open,” *IET Elec. Pow. Appl.*, **15**(7), pp. 847–860, (2021) DOI: 10.1049/elp2.12064

[24] R. Kianinezhad, B. Nahid-Mobarakeh, L. Baghli, et al, “Modeling and control of six-phase symmetrical induction machine under fault condition due to open phases,” *IEEE Trans. Ind. Electron*, **55**(5), pp. 1966–1977, (2008) DOI: 10.1109/TIE.2008.918479

[25] L. Xu, H. Ren, T. Jiang et al., “Minimum copper loss fault-tolerant control of zero phase shift dual three-phase spmsm by using reduced-order transformation matrices,” *IEEE Trans. Energy Convers.*, 2024 DOI: 10.1109/TEC.2024.3385010

[26] F. Rezaee-Alam, A. Hamidi, and M. Hosseini, “A new hybrid analytical model based on winding function theory for analysis of unbalanced two-phase induction motors,” *Scientia Iranica*, 2022 DOI: 1 10.24200/SCI.2022.57654.5348

[27] D. N. Zmood and D. G. Holmes, “Stationary frame current regulation of pwm inverters with zero steady-state error,” *IEEE Trans. Pow. Electron*, **18**(3), pp. 814-822, (2003) DOI: 10.1109/TPEL.2003.810852

[28] A. Akhbari and M. Rahimi, “Performance and stability analysis of single-phase grid-connected inverters used in solar photovoltaic systems,” *Scientia Iranica*, **26**(3), pp. 1637–1651 (2019) DOI: 10.24200/SCI.2017.4384

Table1 The electrical parameters of the six-phase PMSM)

Fig. 1: Six-phase winding configuration

Fig. 2: The phase and transformed currents when only i_α and i_β are non-zero, (a) i_α, i_β and (b) phase currents

Fig. 3: The phase and transformed currents when only i_{z1} and i_{z2} are non-zero, (a) i_{z1}, i_{z2} and (b) phase currents

Fig. 4: The phase and transformed currents when only i_{o1}, i_{o2} are non-zero, (a) i_{o1}, i_{o2} and (b) phase currents

Fig. 5: Six-phase winding configuration with one OC fault at Phase C2

Fig. 6: Model of the faulty six-phase machine with one OC at Phase C2

Fig. 7: Six-phase machine model in $\alpha\beta$ sub-plane with one OC at phase C2 in terms of substitute variables

Fig. 8: Model of six-phase machine with one OC at phase C2 and (a) isolated and (b) connected star points, (a) isolated star points, (b) connected star points

Fig. 9: The cross-section of the dual-star PMSM; the coil directions and phases are shown by letters on the coil sides

Fig. 10: The block diagram of the controller based on the dedicated transformation for the machine with two grounded star points and one OC at Phase C2; (a) the control structure, (b) the feed-forward network, and(b) single-phase controller applied for the control of the zero-axis currents ($L_D = L_d + M_d$ and $L_Q = L_q + M_q$)

Fig. 11: Simulation results with phase C2 at OC, (a) zero-axis currents are supplied at 0.1, 0.15, and 0.2 s to the machine with grounded star points, (b) the feed-forward voltages corresponding to the phase leakage inductance and resistance (equation (41)) are supplied at 0.1, and 0.2 s, respectively, to the machine with connected star points

Fig. 12: Simulation results for the step response of the Q-axis current with phase C2 at OC while all other reference currents are set to zero with isolated neutral points; (a) original leakage inductance (b) reduced leakage inductance

Fig. 13: Switching from minimum-loss to maximum-torque strategy at 0.1 s by injecting proper zero-axis currents found by optimization with isolated and connected star points

Table1 The electrical parameters of the six-phase PMSM)

nominal power voltage	P_{nom}	800 W
nominal phase voltage	V_{nom}	62.5 Vrms
nominal phase current	I_{nom}	7 Arms
nominal torque	I_{nom}	8 N.m
d-axis inductance	L_{d}	5.5 mH
q-axis inductance	L_{q}	6.1 mH
PM flux linkage	ψ_{PM}	70.5 mV.s
d-axis mutual inductance	M_{d}	1.7 mH
q-axis mutual inductance	M_{q}	2.7 mH
phase resistance	r	1.0
leakage inductance	L_{l}	3.8 mH

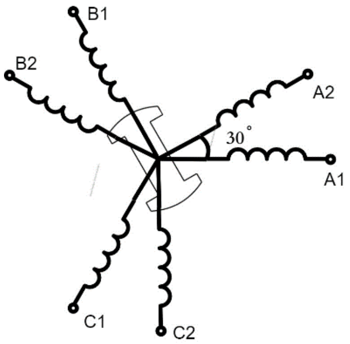

Fig. 1: Six-phase winding configuration

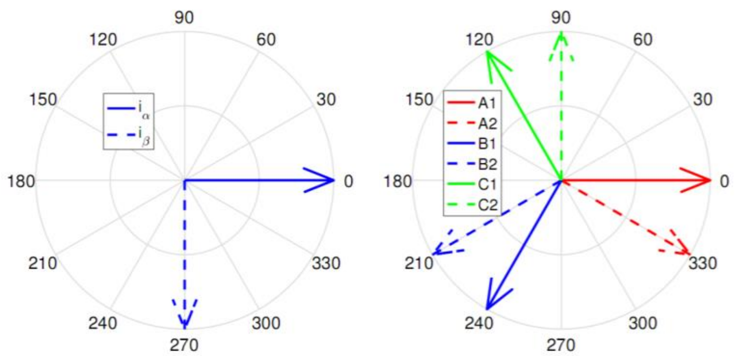

(a) i_α, i_β (b) phase currents

Fig. 2: The phase and transformed currents when only i_α and i_β are non-zero

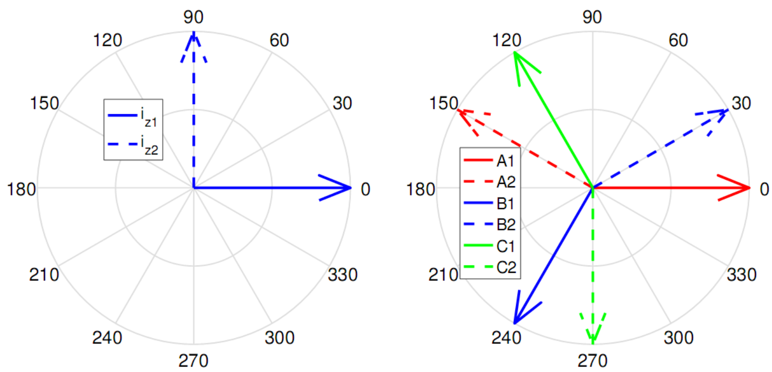

(a) i_{z1}, i_{z2} (b) phase currents

Fig. 3: The phase and transformed currents when only i_{z1} and i_{z2} are non-zero

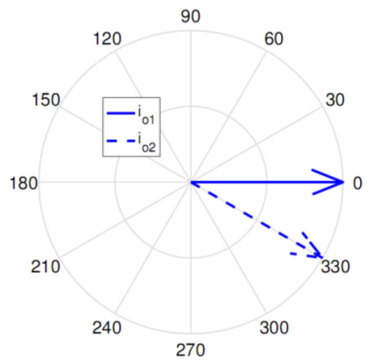

(a) i_{o1}, i_{o2}

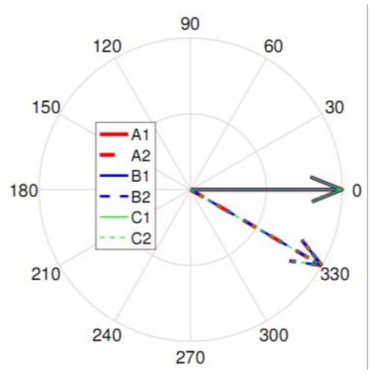

(b) phase currents

Fig. 4: The phase and transformed currents when only i_{o1}, i_{o2} are non-zero

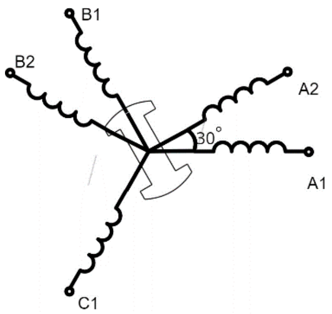

Fig. 5: Six-phase winding configuration with one OC fault at Phase C2

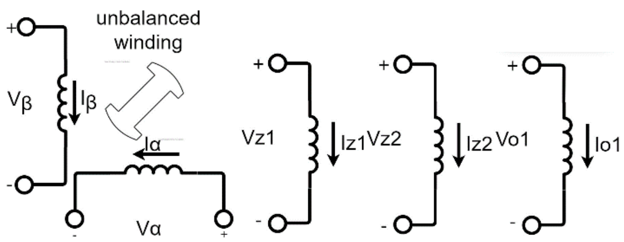

Fig. 6: Model of the faulty six-phase machine with one OC at Phase C2

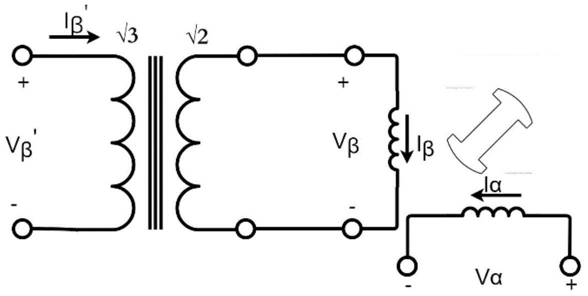

Fig. 7: Six-phase machine model in $\alpha\beta$ sub-plane with one OC at phase C2 in terms of substitute variables

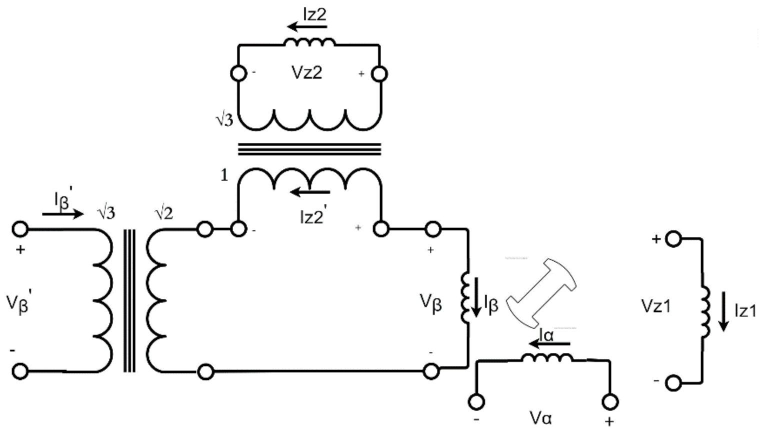

(a) isolated star points

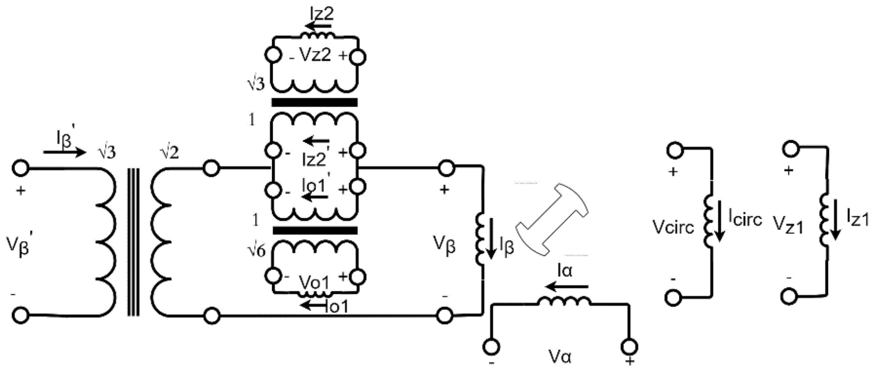

(b) connected star points

Fig. 8: Model of six-phase machine with one OC at phase C2 and (a) isolated and (b) connected star points

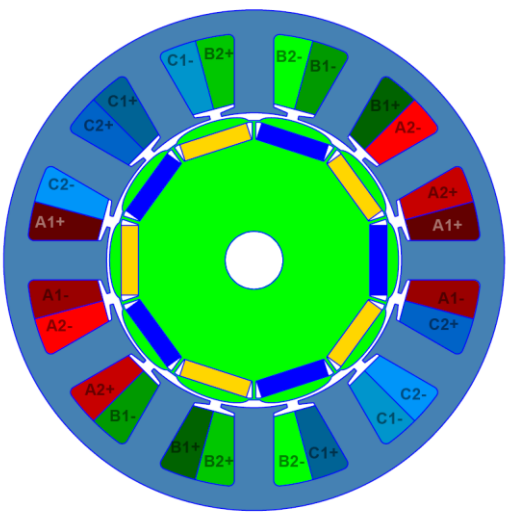

Fig. 9: The cross-section of the dual-star PMSM; the coil directions and phases are shown by letters on the coil sides

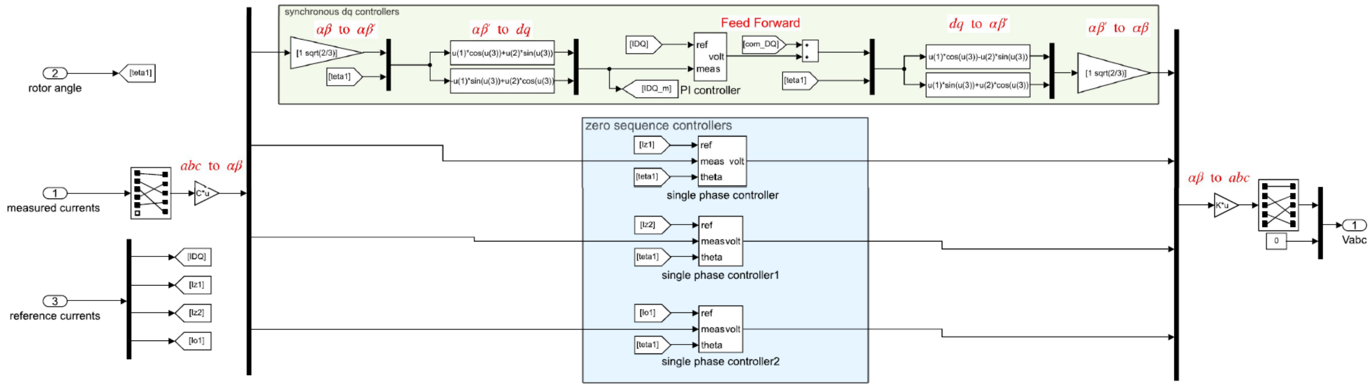

(a) control structure

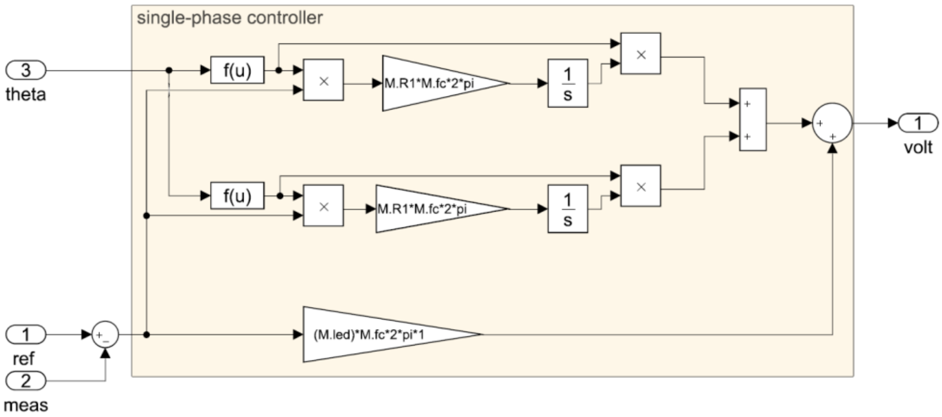

(b) single-phase controller

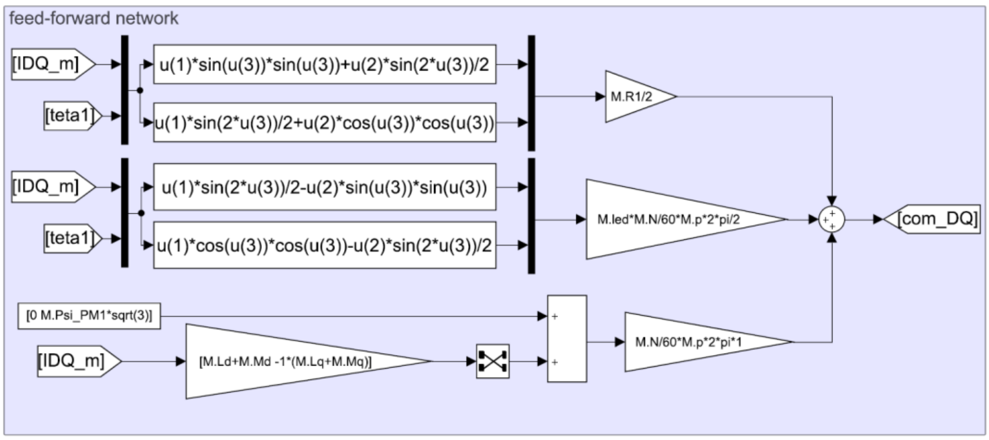

(c) feed-forward voltage

Fig. 10: The block diagram of the controller based on the dedicated transformation for the machine with two grounded star points and one OC at Phase C2; (a) the control structure, (b) the feed-forward network, and(b) single-phase controller applied for the control of the zero-axis currents ($L_D = L_d + M_d$ and $L_Q = L_q + M_q$)

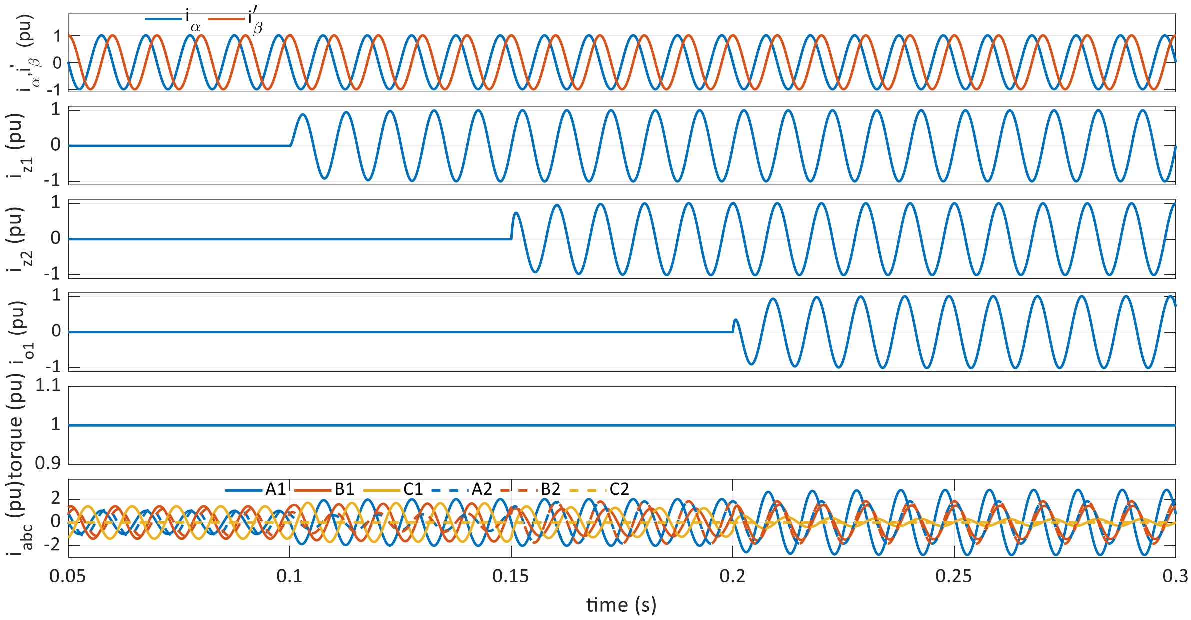

(a) injecting zero sequence currents

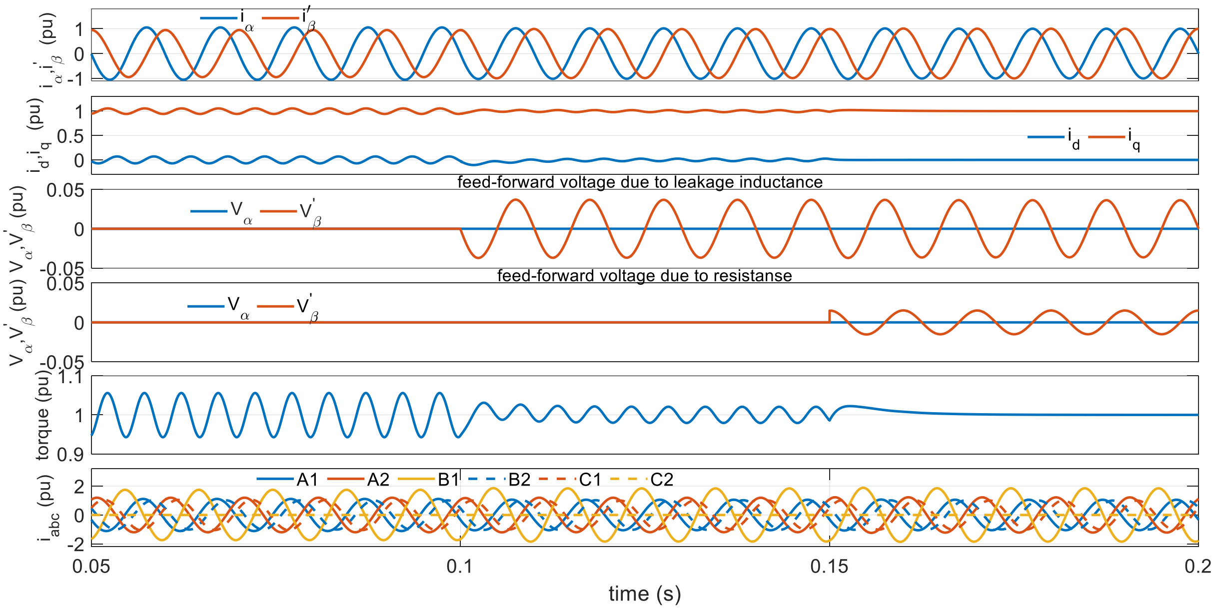

(b) supplying feed-forward voltages

Fig. 11: Simulation results with phase C2 at OC, (a) zero-axis currents are supplied at 0.1, 0.15, and 0.2 s to the machine with grounded star points, (b) the feed-forward voltages corresponding to the phase leakage inductance and resistance (equation (41)) are supplied at 0.1, and 0.2 s, respectively, to the machine with connected star points

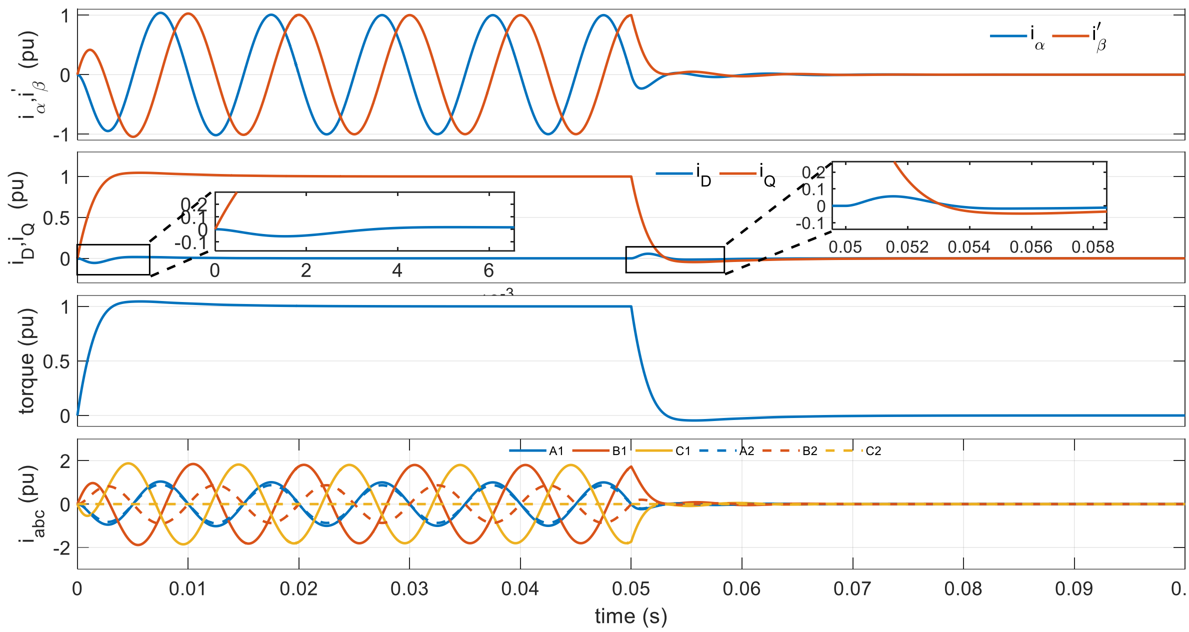

(a) original leakage inductance

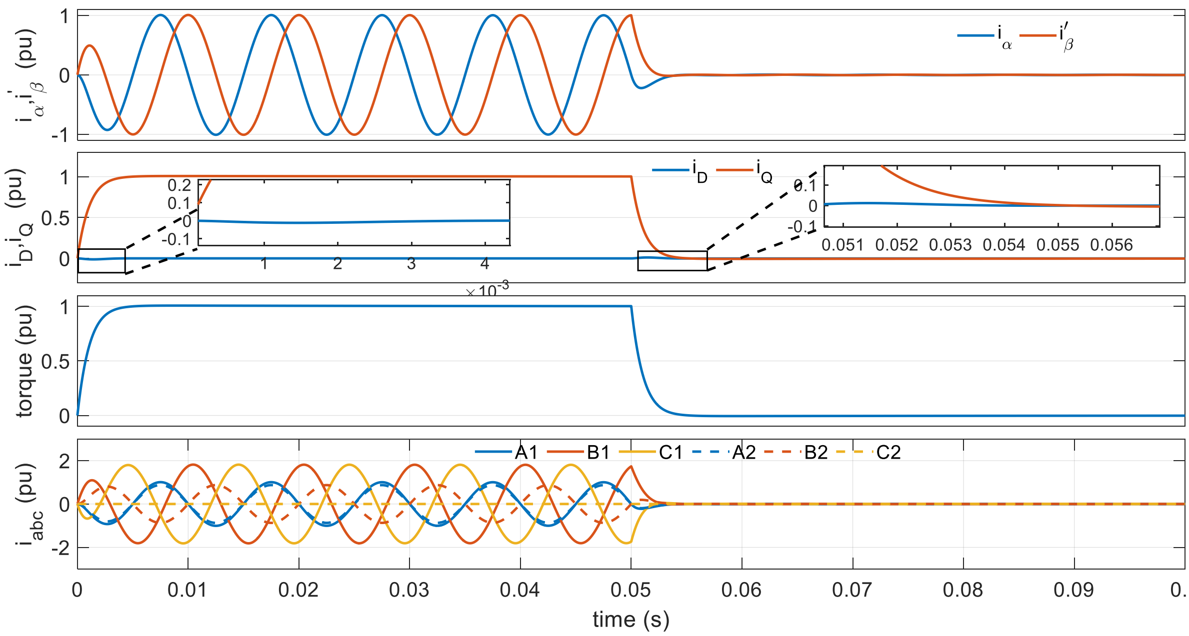

(b) reduced leakage inductance by a factor 10

Fig. 12: Simulation results for the step response of the Q-axis current with phase C2 at OC while all other reference currents are set to zero with isolated neutral points; (a) original leakage inductance (b) reduced leakage inductance

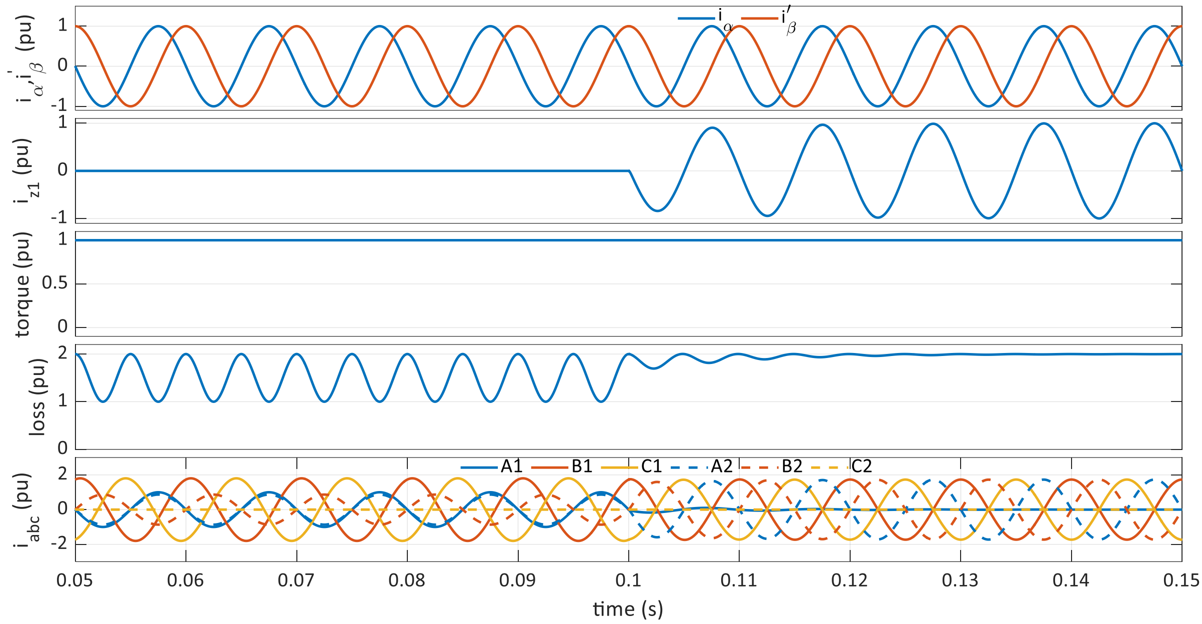

(a) isolated neutral points

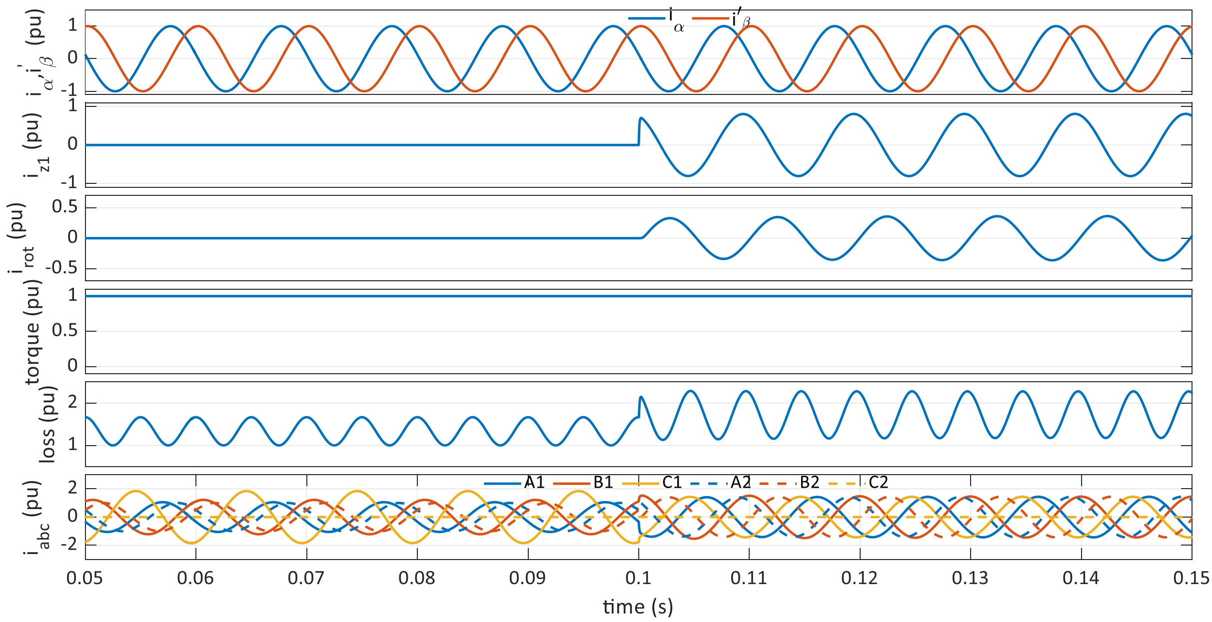

(b) connected neutral points

Fig. 13: Switching from minimum-loss to maximum-torque strategy at 0.1 s by injecting proper zero-axis currents found by optimization with isolated and connected star points

Abdolmajid Abedini Mohammadi received the B.Sc. degree in electrical engineering from Shahrekord University, Shahr-e Kord, Iran, in 2013, the M.Sc. degree in electrical engineering from the Sharif University of Technology, Tehran, Iran, in 2015. In 2022, he obtained his Ph.D. degree in the framework of a joint program between Universität Libre de Bruxelles (ULB), Brussels, Belgium, and Brose Fahrzeugteile SE & Company KG, Würzburg, Germany, within the Drives/Simulation Group. From 2017 to 2018, he was an Electromagnetic Simulation Engineer with the R&D Department of Pars Generator Company, Tehran, Iran. He is currently with AVL software and functions gmbh, Regensburg, Germany, within the e-motor

Simulation Group as an electromagnetic design expert. His research interests include modeling, design, and control of electrical machines for traction applications.

Johan J. C. Gyselinck obtained his M.Sc. and PhD degree in electromechanical engineering at Ghent University (UGent, Belgium) in 1991 and 2000 respectively. From 2000 till 2004 he was postdoctoral researcher and lecturer at the University of Liège (ULiège, Belgium). Since 2004 he is professor at the Université Libre de Bruxelles (ULB, Belgium). His main teaching and research topics are low-frequency numerical magnetics, electrical machines and drives, and renewables (wind and photovoltaics). He is first author or coauthor of some 350 peer-reviewed journal and conference papers.

Adrian-C. Pop received the M. Sc. degree from the Technical University of Cluj-Napoca, Cluj-Napoca, Romania, in 2010 in electrical engineering, and the Ph.D. degree in the framework of a joint program between the Technical University of Cluj-Napoca, and the Université Libre de Bruxelles, Brussels, Belgium, in 2012. Since then, he is with Brose Fahrzeugteile SE & Co. KG, Würzburg, Germany, within the Drives/Simulation Group. His current research is focused on optimal design for cost and performance of brushless AC and DC machines for automotive applications (i.e., light traction, powertrain, chassis, and thermal management) by means of multiphysics analysis starting from the customer-provided requirements and specifications. His past and current subjects of interest include design and optimization of electrical machines and drives (SRMs, PMSMs, and IMs), numerical methods, and hybrid and electrical vehicles.

Dr. Adrian-C. Pop is first author and co-author of some 40 scientific papers and 5 patents. He is member of the IEEE-IES electric machines technical committee.

Samad Taghipour Boroujeni received the B.Sc., M.Sc., and Ph.D. degrees in electrical engineering from the Department of Electrical Engineering, Amirkabir University (Tehran Polytechnic), Tehran, Iran, in 2003, 2005, and 2009, respectively. In 2008, he was a Visiting Scholar with the Electrical Engineering Department, Padova University, Padova, Italy. In 2009, he joined the Department of Engineering, Shahrekord University, Shahrekord, Iran, as an Assistant Professor, where he was serving as an Associate Professor from 2016 to 2020. He had a postdoctoral carrier in 2018-2020 in Lorrain University, Nancy, France in GREEN Lab. He has been a Full Prof. since 2020 at Shahrekord University. His research interests include modeling, design, analysis, optimization, and control of electrical machines, especially variable-speed generators.